The 2022 Starlink geomagnetic storms: global thermospheric response to a high-latitude ionospheric driver

D. D. Billett[1], K. Sartipzadeh[1,2], M. F. Ivarsen[1,3], E. Iorfida[4], E. Doornbos[5], E. C. Kalafatoglu Eyiguler[1], K. Pandey[1], K. A. McWilliams[1]

[1]Institute of Space and Atmospheric Studies, University of Saskatchewan, Saskatoon, SK, Canada
[2]University of Tromsø (UIT) – The Arctic University of Norway, Tromsø, Norwary
[3]Department of Physics, University of Oslo, Oslo, Norway
[4]Aurora Technology B.V. for European Space Agency (ESA), ESTEC, EOP-SME, Noordwijk, The Netherlands
[5]Royal Netherlands Meteorological Institute (KNMI), De Bilt, Netherlands

Key Points:

- Ionosphere-thermosphere observations are examined for the 2022 Starlink geomagnetic storms.
- The thermosphere becomes globally perturbed due to high-latitude magnetosphere-ionosphere forcing.
- The growth, decay, and latitudinal extent of thermospheric density perturbations are investigated.

Corresponding author: D. D. Billett, `daniel.billett@usask.ca`

Abstract

In this study, we present ionospheric observations of field-aligned currents from AMPERE and the ESA Swarm A satellite, in conjunction with high-resolution thermospheric density measurements from accelerometers on board Swarm C and GRACE-FO, for the 3rd and 4th February 2022 geomagnetic storms that led to the loss of 38 Starlink internet satellites. We study the global storm time response of the thermospheric density enhancements, including their growth, decay, and latitudinal distribution. We find that the thermospheric density enhances globally in response to high-latitude energy input from the magnetosphere-solar wind system and takes at least a full day to recover to pre-storm density levels. We also find that the greatest density perturbations occur at polar latitudes consistent with the magnetosphere-ionosphere dayside cusp, and that there appeared to be a saturation of the thermospheric density during the geomagnetic storm on the 4th. Our results highlight the critical importance of high-latitude ionospheric observations when diagnosing potentially hazardous conditions for low-Earth-orbit satellites.

Plain Language Summary

Upwards of a hundred kilometres altitude lies the boundary between Earths atmosphere and space, where the density of air exponentially decreases and many satellites constellations orbit. One of these constellations is Starlink, which provides satellite internet to customers on Earth. In February 2022, a pair of geomagnetic storms stuck Earth shortly after the launch of 49 Starlink satellites, heating the upper atmosphere and causing its density to drastically increase. The higher air density at the initial staging altitude of Starlink caused fatal drag conditions for 38 of the spacecraft, resulting in their destruction a few days later. This paper examines how the air density of the upper atmosphere changed globally in response to space weather energy being deposited at high latitudes during the Starlink geomagnetic storms of February 2022.

1 Introduction

In February 2022, 38 Starlink internet satellites were destroyed shortly after launch as a result of two back-to-back geomagnetic storms on the 3rd and 4th of that month. These storms carried with them an increase to the amount of Poynting flux entering the high-latitude ionosphere of both hemispheres (e.g. C. Y. Huang et al., 2017), leading to

Joule heating and a subsequent perturbation of the thermospheric mass density at low-Earth-orbit (LEO) altitudes (Deng et al., 2009; Wang et al., 2021). Whilst the two storms did ultimately lead to increased thermospheric densities and dangerous orbital drag conditions for Starlink, they would not be considered "extreme", or even "strong", space weather events, as we demonstrate below. The thermosphere experienced a moderate amount of geomagnetic forcing at high-latitudes, which in turn propagated high densities globally, causing the hazardous conditions at Starlink's staging altitude of $\sim$200 km (Dang et al., 2022; Lin et al., 2022; Laskar et al., 2023). The satellites burned up in Earth's atmosphere on 7th February, 2022.

Not only does increased drag lead to potential launch failures such as that seen in February 2022, but it also affects precise orbit determination, satellite lifespans, and collision avoidance (He et al., 2018; Oliveira & Zesta, 2019). Due to LEO altitudes becoming increasingly congested, future costly incidents like the Starlink destruction event are likely to become more frequent. Therefore, it is important that we move towards the real-time monitoring and prediction of the thermospheric mass density, and understanding how it responds to space weather forcing.

The thermospheric effects of the Starlink storms, like other moderate geomagnetic storms, start at Earth's high-latitude ionosphere. Field-aligned-currents (FACs) channel solar wind electromagnetic energy into the ionosphere via magnetospheric reconnection events (e.g. the Dungey cycle; Dungey, 1961), which dissipates through Pedersen currents as Joule heating (Foster et al., 1983). As Joule heating is mostly deposited at E-region altitudes where the Pedersen conductivity is highest (Y. Huang et al., 2012), density perturbations at LEO altitudes are mostly generated by the upwelling of neutral particles and expansion of the thermosphere due to heating pressure from below (Lu et al., 2016). Travelling atmospheric disturbances (TADs) propagate from high to low latitudes as increased pressure drives an equatorward meridional wind (Prölss & Očko, 2000), acting as a vehicle for perturbing globally the thermospheric density (Prölss, 2011).

As alluded to, the Starlink storms were not a major space weather event, yet the thermospheric response to those storms were sufficient to cause major damage to space assets. To what extent was the ionosphere perturbed during these storms, and what was the global thermospheric response? To help answer these questions, we present an analysis of ionospheric and thermospheric observations during the February 2022 Starlink geomagnetic storms. As a measure of the space weather input into the atmosphere, we show FAC measurements from the Active Magnetosphere and Planetary Response Experiment (AMPERE) and Swarm A satellite. For the thermospheric densities, we employ newly processed high-resolution accelerometer measurements from Swarm C and GRACE-FO. Of particular interest is understanding the global extent of thermospheric perturbations in response to a high-latitude ionospheric driver, investigating the growth and decay of density perturbations, as well as their latitudinal distribution.

2 Data

2.1 Thermospheric densities from Swarm-C and GRACE-FO

Thermospheric densities in this study were obtained from the Swarm and Gravity Recovery And Climate Experiment Follow On (GRACE-FO) missions (Friis-Christensen et al., 2008; Kornfeld et al., 2019). In particular, densities used are derived from accelerometers on board Swarm C at an approximate altitude of 450 km and GRACE C at $\sim$500 km. Both satellites fly in a near-polar orbit with inclinations of 87.4° and 89°, respectively.

The ESA Swarm satellites are the 4th ESA Earth Explorer mission, which was launched in November 2013. They are a constellation of 3 identical satellites flying at different altitudes. For all three of the Swarm satellites (A, B and C), calibration of the raw accelerometer measurements has proven difficult due to unforeseen and/or underestimated non-geophysical perturbations (Siemes et al., 2016). Swarm C proved to contain the least number of disturbances and strongest signal-to-noise ratio of the three satellites, thus making it the primary focus of neutral density retrieval efforts over the years. Additionally, densities derived from on-board GPS observations, at a low temporal resolution, have helped greatly in higher-resolution accelerometer calibration efforts (Visser & van den IJssel, 2016; van den IJssel et al., 2020). Swarm C accelerometer measurements now provide good thermospheric density estimations at a 10 second temporal resolution, allowing for high-latitude density perturbations to be effectively decoupled from those low latitudes. We therefore utilise Swarm C accelerometer derived thermospheric densities in this study, as they provide a vast spatio-temporal resolution improvement over GPS densities and allow for the effects of high-latitude geomagnetic energy input to be investigated more rigorously (Iorfida et al., 2023).

GRACE-FO, the successor to the GRACE mission (Tapley et al., 2004) on near-identical hardware, is a twin-satellite mission launched in 2018. Recently, GRACE-FO accelerometer measurements for satellite C of the pair (the other being GRACE D, which unfortunately produced poorer accelerometer data after launch; McCullough et al., 2019) have been released (Siemes et al., 2023), building upon nearly two decades of calibration efforts for the original GRACE, CHAllenging Mini satellite Payload (CHAMP), and Gravity Field and Steady-State Ocean Circulation Explorer (GOCE) satellites (Bruinsma et al., 2004; Doornbos, 2012; Mehta et al., 2017; March et al., 2021). Like Swarm C, thermospheric densities from GRACE-FO are at a 10 second temporal resolution.

2.2 Field aligned currents from Swarm A and AMPERE

We utilise FAC measurements from the AMPERE campaign (Anderson et al., 2014) and Swarm A satellite. FAC's carry the Poynting flux that is mostly dissipated as Joule heating in the atmosphere (Billett et al., 2023), thus their magnitude and spatial extent act as a key parameter in evaluating high-latitude ionospheric driving of any potential thermospheric density enhancements.

Swarm A flies as a satellite pair with Swarm C at the same altitude, separated by 1.4° in longitude. FAC estimations are derived from the on-board vector fluxgate magnetometer (Leger et al., 2009) utilising Ampère's law along with models to remove the terrestrial magnetic field component (Lühr et al., 2015). The Swarm FAC data product has a temporal resolution of 1 second, upon which we apply running mean and Savitsky-Golay filters with 20 second half-window sizes to remove small-scale perturbations and noise.

AMPERE produces high-latitude FAC estimations based on magnetometer observations from the Iridium communications constellation. FAC estimates are available on a 1-degree geomagnetic latitude by 1 hour magnetic local time grid, sampled from a spherical harmonic fit applied to available magnetometer measurements (after subtraction of Earth's main field) (Waters et al., 2020). AMPERE FAC maps are produced at a nominal 10-minute resolution. For the purposes of comparing Swarm A and AMPERE data later in this paper, the AMPERE time intervals shown correspond to average polar pass time of Swarm A, rounded to the nearest 10 minutes.

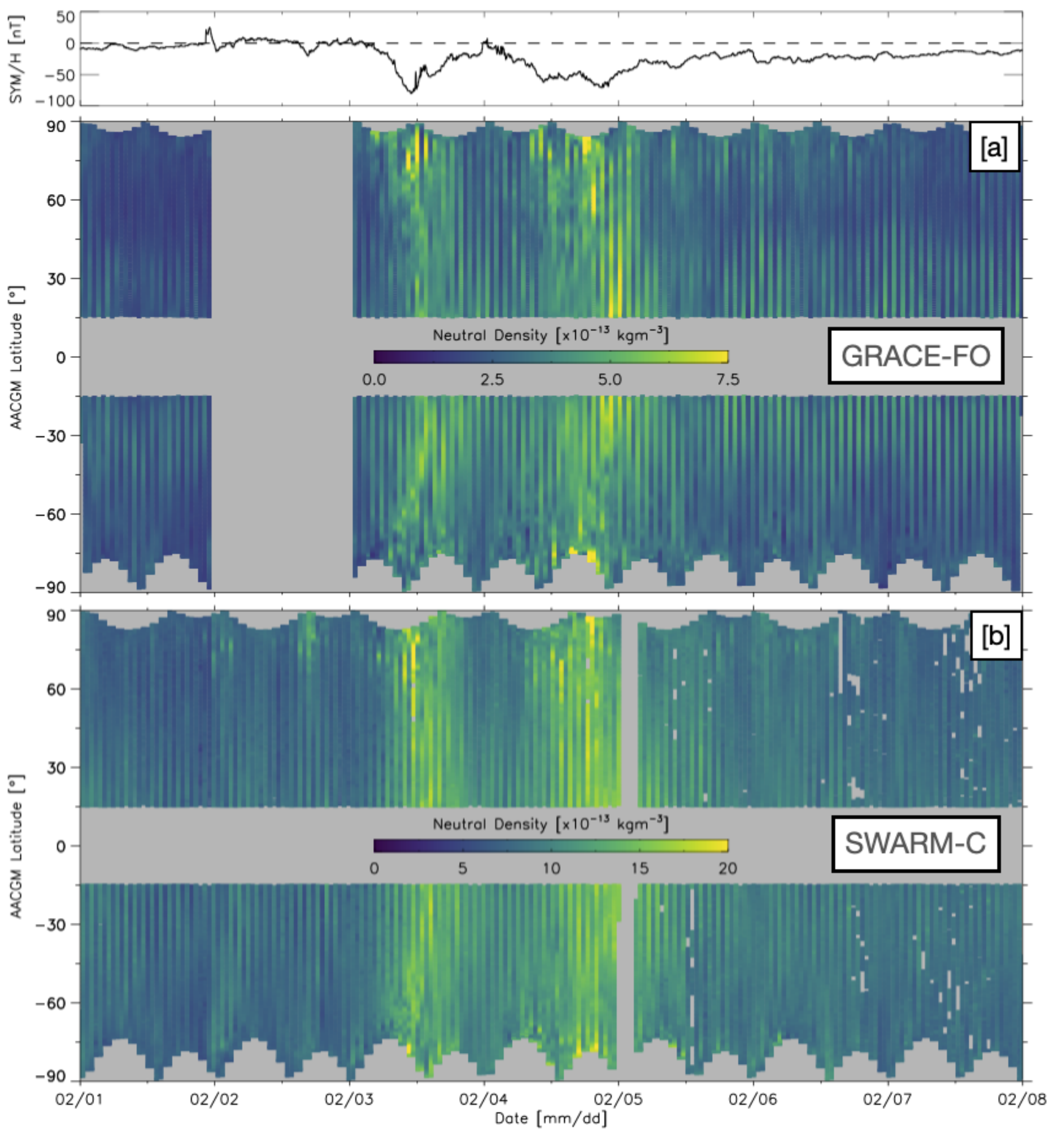

Figure 1. Thermospheric conditions between 1st and 7th February 2022. [Top] 1-minute SYM-H index, [a] Thermospheric neutral density as a function of AACGM latitude and time from GRACE-FO, [b] Densities from Swarm C.

3 Results and Discussion

3.1 Thermospheric density response and decay

Figure 1 presents an overview of the days surrounding the Starlink satellite launch on 3rd February, 2022. The top panel shows the 1-minute geomagnetic SYM-H index, obtained from NASAs OMNIWeb service, whilst panels [a] and [b] show the thermospheric neutral densities measured by GRACE-FO and Swarm C, respectively. The neutral densities are shown in terms of Altitude Adjusted Corrected Geomagnetic (AACGM; Shepherd, 2014) latitude versus time, with periodic gaps near ±90° illustrating the offset of the geomagnetic pole from that of the geographic in both hemispheres. As both GRACE-FO and Swarm C have near-polar orbits in geographic coordinates, coverage above ±80° AACGM latitude is poorer in the southern hemisphere compared to north. As AACGM coordinates are not defined for equatorial latitudes, latitudes between -15° to +15° are not considered. Note that each "half orbit" is shown sequentially, giving the appearance of periodic increases and decreases of the neutral density as the satellite crosses the dayside (higher density), and then the nightside (lower density). GRACE-FO data was unavailable on 2nd February, 2022.

The SYM-H index shown in Figure 1 displays a distinct negative excursion to ∼-80 nT on 3rd February 2022, the day of the Starlink launch. Storm magnitude classifications vary greatly within the literature, however, a storm of SYM-H magnitude as seen during this event would be generally considered "weak" or "moderate" (Hutchinson et al., 2011; Richardson & Cane, 2012; Iong et al., 2022). Concurrent with the 3rd February storm are global scale enhancements of the thermospheric neutral density, captured by both GRACE-FO and Swarm C at altitudes of ∼500 km and ∼460 km, respectively. Note that the colour scales on Figure 1[a] and [b] are different, owing to the normal exponential drop of neutral density with increasing altitude in the thermosphere. The peak neutral density, seen by both GRACE-FO and Swarm C, is at around 80° AACGM latitude in the northern hemisphere. We attribute this high latitude density peak to geomagnetic energy input from the magnetosphere in the form of Joule heating into the ionospheric cusp region (Lühr et al., 2004; Knipp et al., 2011; Billett et al., 2021).

A second geomagnetic storm, longer lasting than the one on 3rd February but of a similar SYM-H magnitude, occurred on 4th February 2022, one day after the Starlink launch. There is another global response of the thermospheric neutral density on the 4th, including an equatorward motion of density enhancements from high northern and southern latitudes over the course of the day, most apparent in the GRACE-FO measurements. This motion is consistent with TAD propagation, and modelling of the same event (Lin et al., 2022; Laskar et al., 2023).

To evaluate the growth and decay of the thermospheric neutral density in response to the geomagnetic storms of the 3rd and 4th February, 2022, Figure 2 shows the hourly

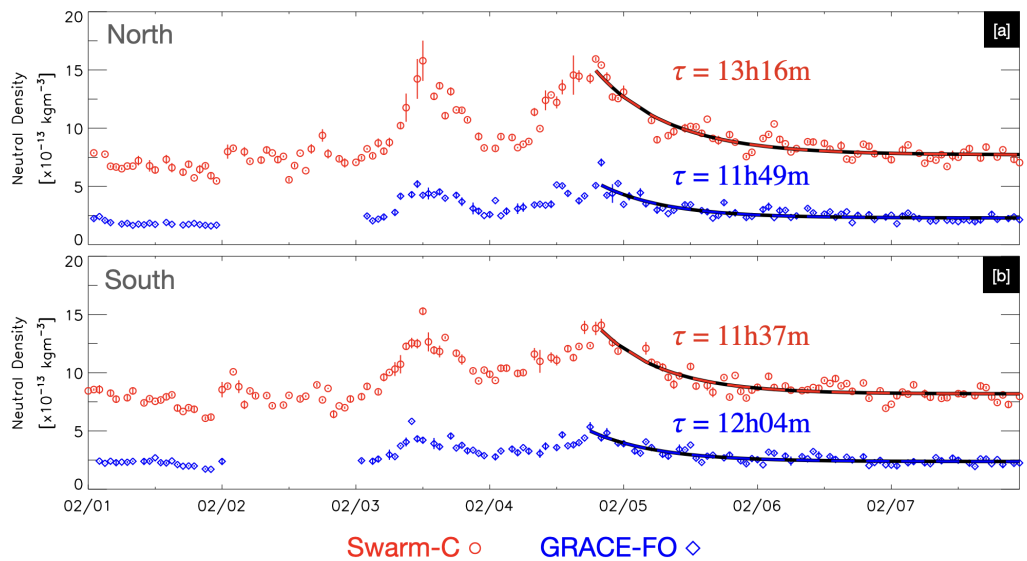

Figure 2. Mean thermospheric neutral densities between 60° and 70° AACGM latitude from 1st and 7th February 2022, measured by GRACE-FO and Swarm C. [a] Northern hemisphere, [b] Southern hemisphere. Exponential decay curves are fitted from the second peak of each time series onwards, with e-folding times for each shown.

averaged densities from GRACE-FO and Swarm C between 60° and 70° AACGM latitude, in the northern [a] and southern [b] hemispheres, respectively. The latitude range was chosen to ensure similar satellite coverage in both hemispheres (owing to the poorer polar coverage in the south), whilst being at a latitude high enough to capture magnetospheric energy inputs due to the geomagnetic storms (i.e. the auroral zone) reasonably soon after they occur. The curves from 4th February onwards are exponential decay least-square fits in the form $\rho(t) = ae^{-t/\tau}$+b, where $\rho(t)$ is the neutral density as a function of time, a and b are fit constants, and τ is the e-folding time. τ is strictly the time taken for the thermospheric density to decrease by a factor of $1/e$, which we use as representative of the time required for the thermosphere to "recover" after the geomagnetic storm on 4th February. The root-mean-square errors (RMSE) of the exponential fits, as a percentage of the mean of the data that was fitted, are 7.6%/6.7% for Swarm (north and south, respectively), and 15.9%/11.8% for GRACE-FO.

Both GRACE-FO and Swarm C measured two distinct neutral density peaks in the auroral zones of both hemispheres (Figure 2a and b), in response to the geomagnetic storms on the 3rd and 4th February, 2022. These time series, averaged over the latitude range 60-70°, are broadly similar to the global orbit averaged time series shown by Lin et al. (2022) for Swarm A, as well as the MAGE, TIEGCM and DTM model outputs. The storm-time density in this latitude range was 1.9% and 2.8% higher in the southern hemisphere compared to the north at GACE-FO and Swarm C altitudes, respectively. This hemispheric difference is rather small considering that the southern hemisphere is in local summer, which should result in a significantly larger overall density than the winter (northern) hemisphere (Ercha et al., 2012). It has previously been seen that there is a northern hemisphere preference for increased magnetospheric energy input when compared to the south (Pakhotin et al., 2021), which would result in a density asymmetry due to Joule heating.

Other hemispheric asymmetries in Figure 2 are present. For example, the density trough around midnight on the 4th of February between the two storm peaks is deeper in the northern hemisphere compared to the south for the same spacecraft. This would imply a quicker decay time for the enhanced neutral density to return to background levels in the northern hemisphere after the storm on 3rd February. τ values calculated from the peak of the 2nd storm onwards, however, do not indicate a faster northern hemisphere recovery for the second storm. τ varies between spacecrafts and hemispheres, ranging from 11h37m to 13h16m, but the decay time from Swarm C in the northern hemisphere is significantly longer than the rest, which vary by around 30 minutes. τ for for Swarm C in the north is 1 hour 12 minutes longer than the next closest τ, which could mean that the density perturbation in the northern hemisphere around 460 km is larger than that in other regions, that the thermosphere there is more "sluggish" in returning to pre-storm levels, or a combination of both conditions. As SYM-H takes several days to return to values near zero after the storm on 4th February (Figure 1), it is also possible there is persistent Joule heating that lingers and causes the neutral density to not fully return to quiet-time levels (Zhou et al., 2007). We note that because the RMSE of the exponential fit for Swarm in the northern hemisphere was 7.6% (approximately 1 hour error in τ), its longer e-folding time may be within error tolerances of the others. The apparent quick thermospheric decay time after the first storm, on 3rd February, may be due to enhanced nitric oxide cooling associated with coronal mass ejection (CME) driven storms (Knipp et al., 2017; Licata et al., 2022), although an exact τ cannot be determined due to the onset of the second storm. Overall decay times presented here are consistent with

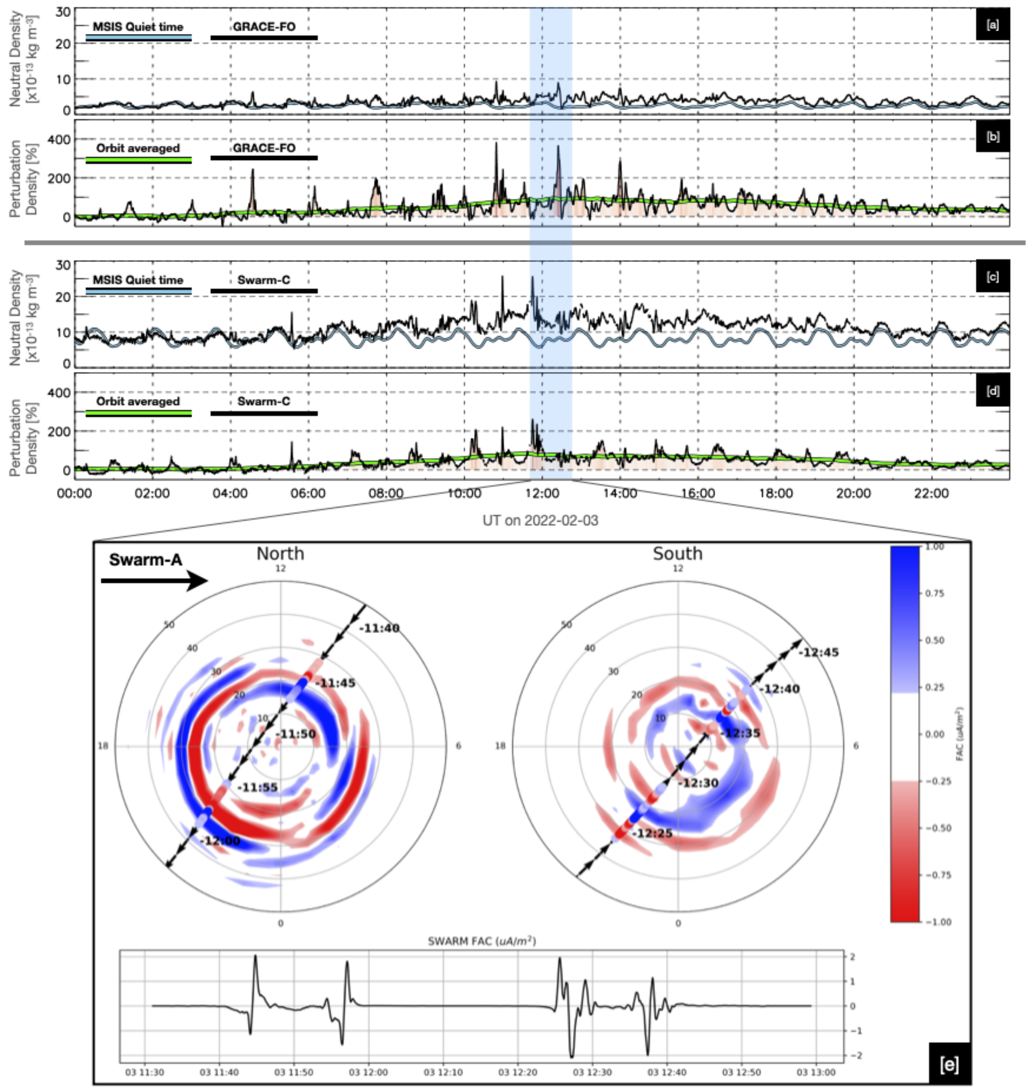

Figure 3. Thermosphere/ionosphere conditions on 3rd February 2022. [a] and [c]: Time series of measured thermospheric densities from GRACE-FO [a] and Swarm C [c], with MSIS quiet time estimations. [b] and [d]: Perturbation thermospheric densities from GRACE-FO [b] and Swarm C [d], with orbit averaged values underlain. [e] AMPERE and Swarm A FAC measurements from within the shaded region.

those presented in the statistical study by Zesta and Oliveira (2019), and likely vary somewhat with local time (e.g. Weimer et al., 2023).

3.2 Disturbance thermospheric densities and ionospheric drivers

We now discuss the high-latitude ionospheric conditions responsible for driving the globally enhanced thermospheric densities on the 3rd and 4th February 2022. Figure 3a and c shows neutral density measurements from GRACE-FO and Swarm C on 3rd February, 2022, accompanied by estimations of the "quiet time" density from the Naval Research Laboratory Mass Spectrometer Incoherent Scatter radar model (NRLMSIS 2.0, shortened to "MSIS" in this study; Emmert et al., 2021). Ap = 3 as MSIS input was chosen to represent "quiet" geomagnetic conditions for the purpose of this study (Joselyn, 1989), which was found to closely resemble the GRACE-FO and Swarm C measurements on the two days prior to the 3rd of February storm. Figure 3b and d show perturbation neutral densities derived by subtracting the quiet time MSIS estimations from the satellite measurements. Orbit averaged perturbation densities are additionally shown here, calculated using a running mean window of size equal to the respective satellites orbital period. Figure 3e shows global AMPERE and local Swarm A FAC measurements during the shaded interval. Overlain black arrows are Swarm A's trajectory over the northern and southern hemisphere high-latitude regions, extending to 50° colatitude (40° AACGM latitude). Swarm A data is shown both as coloured circles over the AMPERE data, as well as a time series. Blue (positive) FAC values are downward (into) in the northern hemisphere and upward (out of) in the south, and vice versa for red.

The negative excursion of SYM-H signifying the start of the storm on 3rd February (Figure 1) begins at ∼05:00UT. It is from approximately then that the neutral density measurements from GRACE-FO and Swarm C begin to deviate from MSIS estimations (Figure 3a and c). Other than the deviation from quiet time baselines, MSIS appears to capture latitudinal and local time variability of the satellite densities well. The deviation is clearer in the perturbation densities (Figure 3b and d), showing that those at both ∼460 km and ∼500 km altitude become enhanced at approximately the same time. The perturbation densities also reveal that both GRACE-FO and Swarm C measure peaks at around the same time, within the highlighted region at 12:00UT, giving a time lag of ∼7 hours between storm onset and peak density perturbation. The maximum single-point perturbation density measurement and orbit averaged perturbation density was 380%/96% for GRACE-FO, respectively, and 260%/84% for Swarm C. We note that although the orbit averaged density perturbation presented here is similar to that determined by other studies for the Starlink storms (Lin et al., 2022; Dang et al., 2022), the moment-to-moment densities at both GRACE-FO and Swarm C altitudes often greatly exceed the average, especially at high latitudes.

AMPERE and Swarm A FACs are shown in Figure 3e for the shaded interval in panels a-d, roughly coinciding with the time of peak perturbation density. AMPERE and Swarm A are in good agreement with each other. The northern hemisphere FAC pattern extended further equatorward than in the south and contained higher current magnitudes (which would result in more Joule heating). However, both hemispheres display FACs indicative of active magnetospheric forcing. The northern hemisphere FAC is more akin to a "classical" FAC picture than the south, with clearly structured R1 and R2 currents on both the dawn and dusk sides (Iijima & Potemra, 1978).

Figure 4a-d shows thermospheric conditions for 4th February 2022, one day after the Starlink launch and the day of the second geomagnetic storm. The SYM-H onset of this storm was at approximately 01:00 UT, with a peak negative excursion reached at ∼21:00 UT (Figure 1). The peak perturbation neutral density observed by both GRACE-FO and Swarm C occurred around 19:00 UT, an 18 hour lag from storm onset. This much longer lag time, compared to the 3rd, is probably due to the long ∼20 hour main phase indicated by the SYM-H index. It is interesting that the peak perturbation density on the 4th occurred 1-2 hours before the peak SHM-H negative excursion, as it implies there is perhaps a thermospheric density "saturation" point that is based on the duration of the storm main phase, and/or the magnitude of the storm itself. The peak single-point perturbation density measurement and orbit averaged perturbation density was higher on the 4th compared to the 3rd, 476%/125% respectively for GRACE-FO. Swarm C measured several very large density perturbations over a 5-minute period at 18:50 UT which were not flagged as anomalous in the data quality flags, resulting in a maximum single-point perturbation density measurement of 510%. We treat this as anomalous as the maxima during the preceding and proceeding peaks were under 200%, and because the thermospheric density is highly unlikely to vary by so much so quickly. The peak orbit-averaged perturbation density measured by Swarm C was 107% (excluding anomalous points), higher than that seen on the 3rd of February.

The orbit averaged densities from GRACE-FO and Swarm C were considerably higher on the 4th of February compared to the 3rd, by 29% and 23%, respectively. We attribute this difference to the global extent of density enhancements that each storm produced.

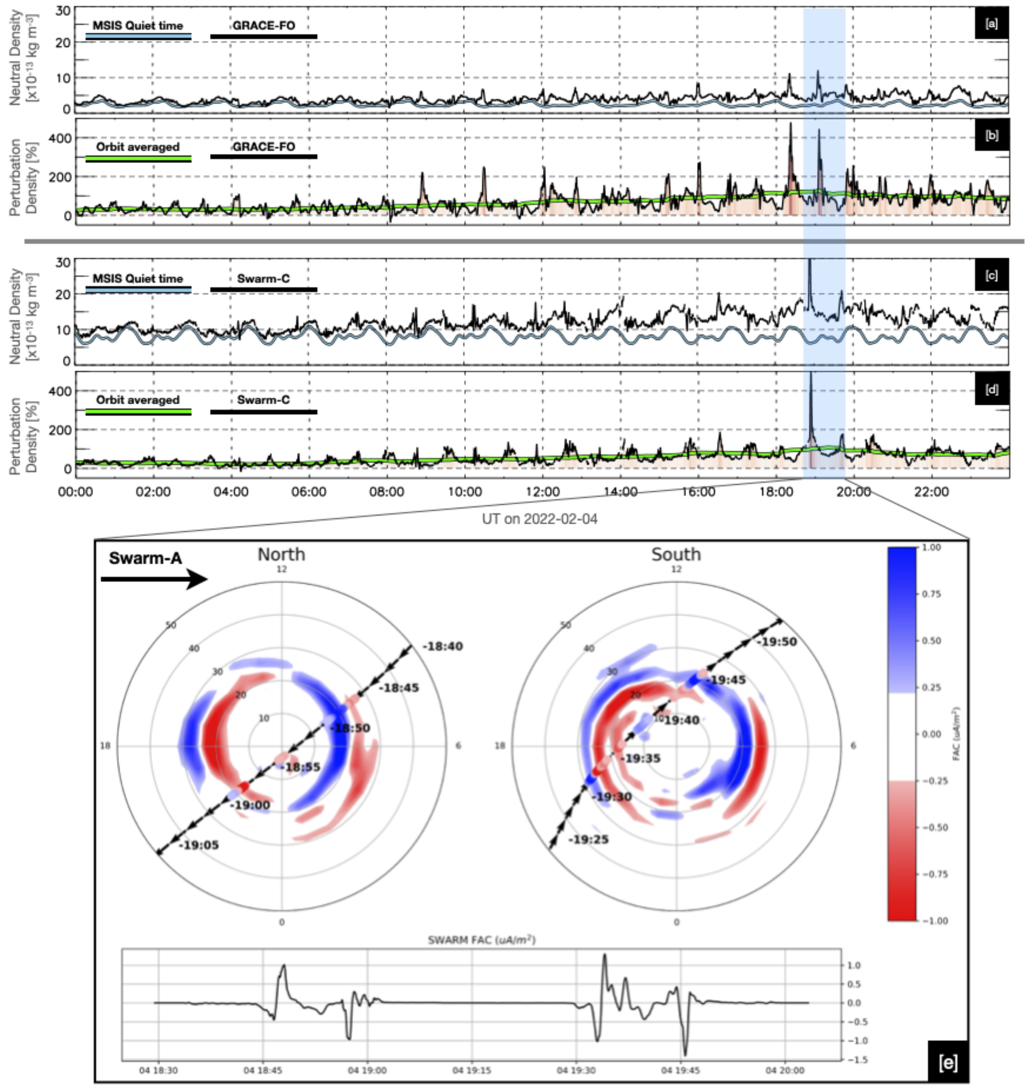

Figure 4. Same format as Figure 3, but for 4th February 2022.

Figure 1a and b shows that the storm on the 4th resulted in density perturbations propagating to low latitudes, whilst enhancements on the 3rd were mostly at northern hemisphere high latitudes. The density asymmetry seen on the 3rd is not seen on the 4th, which may be related to the aformentioned FAC asymmetry (Figure 3e). On the 4th, the northern and southern hemisphere FACs observed by AMPERE and Swarm A are more symmetric (Figure 4e), which would result in more symmetric Joule heating, and thus a more symmetric distribution of density enhancements and TAD propagation. The latter causes an "intersection" of TADs at low latitudes, driving significant density enhancements there (e.g. those seen on the 4th February in Figure 1) (Pham et al., 2022).

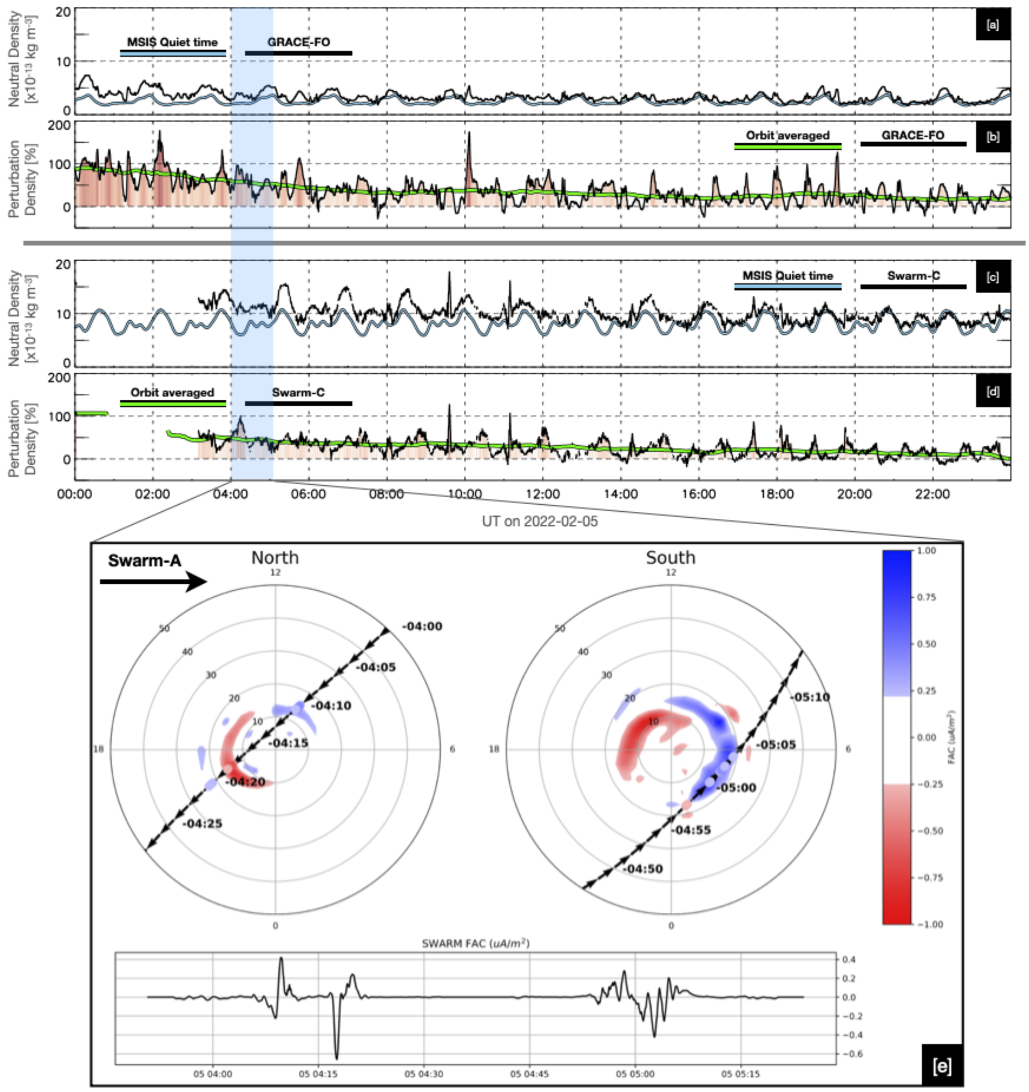

Figure 5. Same format as Figure 3, but for 5th February 2022.

Thus, the asymmetric FACs on the 3rd would produce asymmetric TAD propagation, in agreement with recent modelling work (Zhu et al., 2023; Hong et al., 2023).

Next, we demonstrate that the thermospheric enhancements were significantly longer lived than the storm itself. Figure 5 is in the same format as Figures 3 and 4, but showing the 5th of February 2022 (the day after the second storm, two days after the Starlink launch). There were no additional storms on this day according to the SYM-H index (Figure 1) and the densities observed by GRACE-FO and Swarm C gradually decreased throughout the day, eventually returning close to the MSIS quiet-time baseline. AMPERE and Swarm A FAC's are shown for the highlighted times around 04:30 UT (Fig-

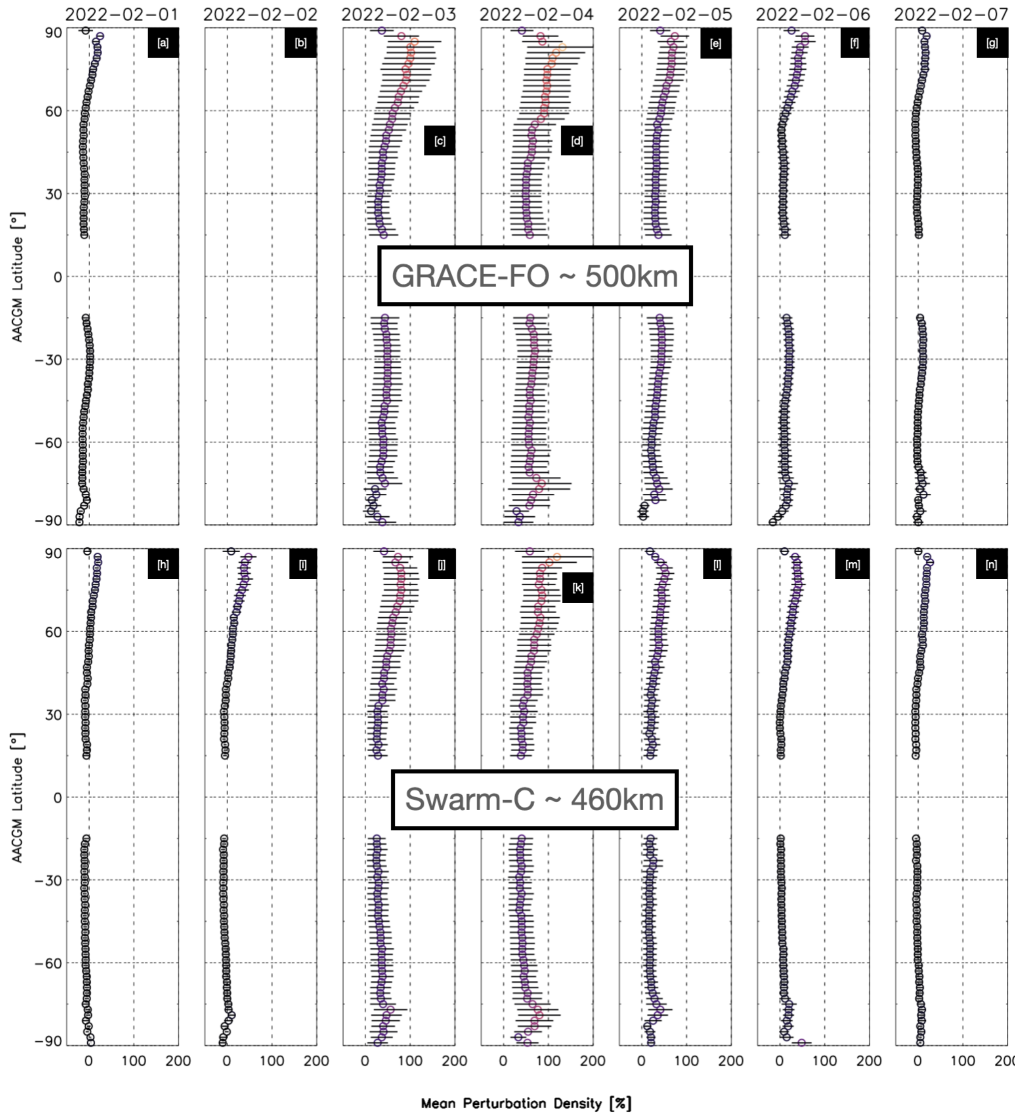

Figure 6. Latitude profiles of the mean thermospheric density from GRACE-FO [a-g] and Swarm C [h-n], for 1st - 7th February 2022.

ure 5e), showing that the FAC equatorward extent and magnitude where drastically reduced compared to the previous two storm days. Figure 5 illustrates that the thermosphere after the storms took at least a full day to return to near-quiet-time density levels (with e-folding times given in Figure 2), whilst the ionospheric driving conditions decayed much faster. FAC reconfiguration timescales after changes in solar wind driving, and in turn Joule heating reconfiguration times, are typically on the order of 10-150 mins (Anderson et al., 2018; Coxon et al., 2019; Billett et al., 2022).

Finally, we investigated the latitudinal dependence of the perturbation thermospheric density by creating daily mean profiles versus latitude, shown in Figure 6 from 1st to 7th February 2022. The 7th of February is the date on which the failed Starlink satellites burned up on re-entry.

The largest perturbation densities were seen on storm days (Figure 6c, d, j, k), with larger perturbations seen by GRACE-FO compared to Swarm C (500 km/460 km average altitude, respectively). GRACE-FO measured maximum mean perturbations of 110% and 131% on the 3rd and 4th respectively, compared to Swarm C measurements of 80% and 86%. Maximums from both satellites were in the northern hemisphere, at polar cap latitudes between 75° and 85°. These latitudes are considerably higher than typical auroral latitudes of ∼65°-70°, implying that the peak magnetospheric energy input into atmosphere for these storms is occurring on open magnetic field lines, or close to the open-closed field line boundary. This is a similar result to those presented by R. Liu et al. (2010), C. Y. Huang et al. (2014), Shi et al. (2017), and Wang et al. (2021), who all saw large geomagnetic storm-associated thermospheric density enhancements occurring well within the polar cap. These enhancements have been attributed to Joule heating in the region of enhanced cusp FACs and are likely related to the development of the "cusp density anomaly" (Lühr et al., 2004). The latitudinal width of density enhancements were also smaller in the southern hemisphere compared to north, which is consistent with the statistical distribution of the cusp density anomaly in both hemispheres (H. Liu et al., 2005).

It is noted there were also discernible high latitude perturbations on average during the two days before the first storm (Figure 6a, b, h, i), particularly in the northern hemisphere, even though the geomagnetic activity levels were low (Figure 1). Significant perturbation densities on these days, although much smaller than those on storm days, implies that MSIS underestimates the high-latitude thermosphere to some degree when using Ap = 3 as quiet time input. Alternatively, there may also be lingering thermospheric density enhancements on the 1st and 2nd February due to a minor geomagnetic storm that occurred at the end of January (Berger et al., 2023). Therefore, perturbation densities presented in this study are likely to be overestimations.

4 Summary

We have presented an analysis of the ionosphere-thermosphere conditions which lead to the loss of Starlink internet satellites in February 2022. Discrete geomagnetic storms on the 3rd and 4th February drove increases of the thermospheric mass density, increasing drag on the satellites and leading them to de-orbit on the 7th.

Utilising newly processed high-resolution thermospheric density measurements from Swarm C and GRACE-FO, we have gained new insights into the global extent of density enhancements due to high-latitude ionospheric driving (captured by AMPERE and Swarm A FAC measurements). In particular:

- Thermospheric densities become enhanced globally, but are largest in the high-latitude polar regions above 80° AACGM latitude. The latitudinal distribution of the density perturbations is consistent with magnetospheric energy input into the cusp.
- Density perturbations between the northern and southern hemispheres were more symmetric on the 4th compared to the 3rd. This is consistent with the FAC data from AMPERE, which likewise exhibits stronger hemispherical symmetry on the 4th compared to the 3rd of February.
- Thermospheric density e-folding decay timescales in the auroral zones of both hemispheres were approximately 12 hours, except for Swarm C in the northern hemisphere, which was around 13 hours. The magnitude and extent of FACs reduced much quicker.
- The perturbation thermospheric density on the 4th appears to saturate, with its peak occurring 1-2 hours before the maximum excursion of SYM-H. This may be due to the very long main phase of the 4th of February storm, which lasted around 20 hours.

This study emphasises the importance of capturing high-latitude ionospheric conditions when considering the impact of geomagnetic storms on the thermosphere, which can have dire consequences for LEO assets. These thermospheric storm effects are global in their extent and complex in their growth and decay, whilst their drivers are confined to high latitudes. There is additionally a complex thermospheric interplay between hemispheres, as ionospheric conditions in each can be highly asymmetric. For future analysis and potential real-time monitoring to support LEO satellite launches, capturing the high-latitude ionosphere is imperative.

Acknowledgments

This research was supported by the European Space Agency (ESA) Living Planet Fellowship programme and by the National Sciences and Engineering Research Council of Canada (NSERC). DDB was supported by ESA under the "HLPF-SSA" project and by NSERC under CREATE Grant #479771-20. KM was supported by NSERC Discovery Grant #RGPIN 05472-2017. Data from the ESA Swarm A and C satellites was obtained from `https://swarm-diss.eo.esa.int`. AMPERE data can be plotted and downloaded at `http://ampere.jhuapl.edu/`. The NRLMSIS 2.0 model Fortran code was obtained from `https://map.nrl.navy.mil/map/pub/nrl/NRLMSIS/NRLMSIS2.0/`.

References

Anderson, B. J., Korth, H., Waters, C. L., Green, D. L., Merkin, V. G., Barnes, R. J., & Dyrud, L. P. (2014). Development of large-scale birkeland currents determined from the active magnetosphere and planetary electrodynamics response experiment. *Geophysical Research Letters*, *41*(9), 3017–3025.

Anderson, B. J., Olson, C. N., Korth, H., Barnes, R. J., Waters, C. L., & Vines, S. K. (2018). Temporal and spatial development of global birkeland currents. *Journal of Geophysical Research: Space Physics*, *123*(6), 4785–4808.

Berger, T. E., Dominique, M., Lucas, G., Pilinski, M., Ray, V., Sewell, R., ... Thiemann, E. (2023). The thermosphere is a drag: The 2022 starlink incident and the threat of geomagnetic storms to low earth orbit space operations. *Space Weather*, *21*(3), e2022SW003330.

Billett, D. D., McWilliams, K. A., Perry, G. W., Clausen, L. B. N., & Anderson, B. J. (2022). Ionospheric energy input in response to changes in solar wind driving: Statistics from the SuperDARN and AMPERE campaigns. *Journal of Geophysical Research: Space Physics*, *127*(3), e2021JA030102.

Billett, D. D., McWilliams, K. A., Ponomarenko, P. V., Martin, C. J., Knudsen, D. J., & Vines, S. K. (2023). Multi-scale ionospheric poynting fluxes using ground and space-based observations. *Geophysical Research Letters*, *50*(10), e2023GL103733.

Billett, D. D., Perry, G. W., Clausen, L. B. N., Archer, W. E., McWilliams, K. A., Haaland, S., ... others (2021). The relationship between large scale thermospheric density enhancements and the spatial distribution of poynting flux. *Journal of Geophysical Research: Space Physics*, *126*(5), e2021JA029205.

Bruinsma, S., Tamagnan, D., & Biancale, R. (2004). Atmospheric densities derived from CHAMP/STAR accelerometer observations. *Planetary and Space Science*, *52*(4), 297–312.

Coxon, J. C., Shore, R. M., Freeman, M. P., Fear, R. C., Browett, S. D., Smith, A. W., ... Anderson, B. J. (2019). Timescales of Birkeland currents driven by the IMF. *Geophysical Research Letters*, *46*(14), 7893–7901.

Dang, T., Li, X., Luo, B., Li, R., Zhang, B., Pham, K., ... Wang, Y. (2022). Unveiling the space weather during the starlink satellites destruction event on 4 february 2022. *Space weather*, *20*(8), e2022SW003152.

Deng, Y., Maute, A., Richmond, A. D., & Roble, R. G. (2009). Impact of electric field variability on joule heating and thermospheric temperature and density. *Geophysical Research Letters*, *36*(8).

Doornbos, E. (2012). *Thermospheric density and wind determination from satellite dynamics*. Springer Science & Business Media.

Dungey, J. W. (1961). Interplanetary magnetic field and the auroral zones. *Physical Review Letters*, *6*(2), 47.

Emmert, J. T., Drob, D. P., Picone, J. M., Siskind, D. E., Jones Jr, M., Mlynczak, M. G., ... others (2021). NRLMSIS 2.0: A whole-atmosphere empirical model of temperature and neutral species densities. *Earth and Space Science*, *8*(3), e2020EA001321.

Ercha, A., Ridley, A. J., Zhang, D., & Xiao, Z. (2012). Analyzing the hemispheric asymmetry in the thermospheric density response to geomagnetic storms. *Journal of Geophysical Research. Space Physics*, *117*(8).

Foster, J. C., St.-Maurice, J.-P., & Abreu, V. J. (1983). Joule heating at high latitudes. *Journal of Geophysical Research: Space Physics*, *88*(A6), 4885–4897.

Friis-Christensen, E., Lühr, H., Knudsen, D., & Haagmans, R. (2008). Swarm–an earth observation mission investigating geospace. *Advances in Space Research*, *41*(1), 210–216.

He, C., Yang, Y., Carter, B., Kerr, E., Wu, S., Deleflie, F., ... Norman, R. (2018).

Review and comparison of empirical thermospheric mass density models. *Progress in Aerospace Sciences*, *103*, 31–51.

Hong, Y., Deng, Y., Zhu, Q., Maute, A., Hairston, M. R., Waters, C., … Lopez, R. E. (2023). Inter-hemispheric asymmetries in high-latitude electrodynamic forcing and the thermosphere during the october 8–9, 2012, geomagnetic storm: An integrated data–model investigation. *Frontiers in Astronomy and Space Sciences*, *10*, 1062265.

Huang, C. Y., Huang, Y., Su, Y.-J., Hairston, M. R., & Sotirelis, T. (2017). DMSP observations of high latitude Poynting flux during magnetic storms. *Journal of Atmospheric and Solar-Terrestrial Physics*, *164*, 294–307.

Huang, C. Y., Su, Y.-J., Sutton, E. K., Weimer, D. R., & Davidson, R. L. (2014). Energy coupling during the august 2011 magnetic storm. *Journal of Geophysical Research: Space Physics*, *119*(2), 1219–1232.

Huang, Y., Richmond, A. D., Deng, Y., & Roble, R. (2012). Height distribution of joule heating and its influence on the thermosphere. *Journal of Geophysical Research: Space Physics*, *117*(A8).

Hutchinson, J. A., Wright, D. M., & Milan, S. E. (2011). Geomagnetic storms over the last solar cycle: A superposed epoch analysis. *Journal of Geophysical Research: Space Physics*, *116*(A9).

Iijima, T., & Potemra, T. A. (1978). Large-scale characteristics of field-aligned currents associated with substorms. *Journal of Geophysical Research: Space Physics*, *83*(A2), 599–615.

Iong, D., Chen, Y., Toth, G., Zou, S., Pulkkinen, T., Ren, J., … Gombosi, T. (2022). New findings from explainable SYM-H forecasting using gradient boosting machines. *Space Weather*, *20*(8), e2021SW002928.

Iorfida, E., Daras, I., Haagmans, R., & Strømme, A. (2023). Swarm A and C accelerometers: Data validation and scientific interpretation. *Earth and Space Science*, *10*(2).

Joselyn, J. A. (1989). Geomagnetic quiet day selection. *pure and applied geophysics*, *131*, 333–341.

Knipp, D. J., Eriksson, S., Kilcommons, L., Crowley, G., Lei, J., Hairston, M., & Drake, K. (2011). Extreme poynting flux in the dayside thermosphere: Examples and statistics. *Geophysical Research Letters*, *38*(16).

Knipp, D. J., Pette, D. V., Kilcommons, L. M., Isaacs, T. L., Cruz, A. A., Mlynczak, M. G., ... Lin, C. Y. (2017). Thermospheric nitric oxide response to shock-led storms. *Space Weather*, *15*(2), 325–342.

Kornfeld, R. P., Arnold, B. W., Gross, M. A., Dahya, N. T., Klipstein, W. M., Gath, P. F., & Bettadpur, S. (2019). GRACE-FO: the gravity recovery and climate experiment follow-on mission. *Journal of spacecraft and rockets*, *56*(3), 931–951.

Laskar, F. I., Sutton, E. K., Lin, D., Greer, K. R., Aryal, S., Cai, X., ... others (2023). Thermospheric temperature and density variability during 3–4 february 2022 minor geomagnetic storm. *Space Weather*, *21*(4), e2022SW003349.

Leger, J.-M., Bertrand, F., Jager, T., Le Prado, M., Fratter, I., & Lalaurie, J.-C. (2009). Swarm absolute scalar and vector magnetometer based on helium 4 optical pumping. *Procedia Chemistry*, *1*(1), 634–637.

Licata, R. J., Mehta, P. M., Weimer, D. R., Drob, D. P., Tobiska, W. K., & Yoshii, J. (2022). Science through machine learning: Quantification of post-storm thermospheric cooling. *Space Weather*, *20*(9), e2022SW003189.

Lin, D., Wang, W., Garcia-Sage, K., Yue, J., Merkin, V., McInerney, J. M., ... Sorathia, K. (2022). Thermospheric neutral density variation during the "SpaceX" storm: Implications from physics-based whole geospace modeling. *Space Weather*, *20*(12), e2022SW003254.

Liu, H., Lühr, H., Henize, V., & Köhler, W. (2005). Global distribution of the thermospheric total mass density derived from CHAMP. *Journal of Geophysical Research: Space Physics*, *110*(A4).

Liu, R., Lühr, H., & Ma, S.-Y. (2010). Storm-time related mass density anomalies in the polar cap as observed by CHAMP. In *Annales geophysicae* (Vol. 28, pp. 165–180).

Lu, G., Richmond, A. D., Lühr, H., & Paxton, L. (2016). High-latitude energy input and its impact on the thermosphere. *Journal of Geophysical Research: Space Physics*, *121*(7), 7108–7124.

Lühr, H., Park, J., Gjerloev, J. W., Rauberg, J., Michaelis, I., Merayo, J. M. G., & Brauer, P. (2015). Field-aligned currents' scale analysis performed with the swarm constellation. *Geophysical Research Letters*, *42*(1), 1–8.

Lühr, H., Rother, M., Köhler, W., Ritter, P., & Grunwaldt, L. (2004). Thermospheric up-welling in the cusp region: Evidence from CHAMP observations. *Geophysical Research Letters*, *31*(6).

March, G., Van Den Ijssel, J., Siemes, C., Visser, P. N., Doornbos, E. N., & Pilinski, M. (2021). Gas-surface interactions modelling influence on satellite aerodynamics and thermosphere mass density. *Journal of Space Weather and Space Climate*, *11*, 54.

McCullough, C. M., Harvey, N., Save, H., & Bandikova, T. (2019). Description of calibrated GRACE-FO accelerometer data products (ACT). *Level-1 product version*, *4*.

Mehta, P. M., Walker, A. C., Sutton, E. K., & Godinez, H. C. (2017). New density estimates derived using accelerometers on board the CHAMP and GRACE satellites. *Space Weather*, *15*(4), 558–576.

Oliveira, D. M., & Zesta, E. (2019). Satellite orbital drag during magnetic storms. *Space Weather*, *17*(11), 1510–1533.

Pakhotin, I. P., Mann, I. R., Xie, K., Burchill, J. K., & Knudsen, D. J. (2021). Northern preference for terrestrial electromagnetic energy input from space weather. *Nature communications*, *12*(1), 199.

Pham, K. H., Zhang, B., Sorathia, K., Dang, T., Wang, W., Merkin, V., … others (2022). Thermospheric density perturbations produced by traveling atmospheric disturbances during august 2005 storm. *Journal of Geophysical Research: Space Physics*, *127*(2), e2021JA030071.

Prölss, G. W. (2011). Density perturbations in the upper atmosphere caused by the dissipation of solar wind energy. *Surveys in Geophysics*, *32*, 101–195.

Prölss, G. W., & Očko, M. (2000). Propagation of upper atmospheric storm effects towards lower latitudes. *Advances in Space Research*, *26*(1), 131–135.

Richardson, I. G., & Cane, H. V. (2012). Solar wind drivers of geomagnetic storms during more than four solar cycles. *Journal of Space Weather and Space Climate*, *2*, A01.

Shepherd, S. G. (2014). Altitude-adjusted corrected geomagnetic coordinates: Definition and functional approximations. *Journal of Geophysical Research: Space Physics*, *119*(9), 7501–7521.

Shi, Y., Zesta, E., Connor, H. K., Su, Y.-J., Sutton, E. K., Huang, C. Y., … Oliveira, D. M. (2017). High-latitude thermosphere neutral density response to solar wind dynamic pressure enhancement. *Journal of Geophysical Research: Space Physics*, *122*(11), 11–559.

Siemes, C., Borries, C., Bruinsma, S., Fernandez-Gomez, I., Hładczuk, N., den IJssel, J., ... Visser, P. (2023). New thermosphere neutral mass density and crosswind datasets from CHAMP, GRACE, and GRACE-FO. *Journal of Space Weather and Space Climate*, *13*, 16.

Siemes, C., de Teixeira da Encarnação, J., Doornbos, E., Van Den Ijssel, J., Kraus, J., Pereštỳ, R., ... Holmdahl Olsen, P. E. (2016). Swarm accelerometer data processing from raw accelerations to thermospheric neutral densities. *Earth, Planets and Space*, *68*, 1–16.

Tapley, B. D., Bettadpur, S., Watkins, M., & Reigber, C. (2004). The gravity recovery and climate experiment: Mission overview and early results. *Geophysical research letters*, *31*(9).

van den IJssel, J., Doornbos, E., Iorfida, E., March, G., Siemes, C., & Montenbruck, O. (2020). Thermosphere densities derived from Swarm GPS observations. *Advances in Space Research*, *65*(7), 1758–1771.

Visser, P. N. A. M., & van den IJssel, J. (2016). Calibration and validation of individual GOCE accelerometers by precise orbit determination. *Journal of Geodesy*, *90*, 1–13.

Wang, X., Miao, J., Lu, X., Aa, E., Liu, J., Wang, Y., & Liu, S. (2021). Latitudinal impacts of joule heating on the high-latitude thermospheric density enhancement during geomagnetic storms. *Journal of Geophysical Research: Space Physics*, *126*(7), e2020JA028747.

Waters, C. L., Anderson, B. J., Green, D. L., Korth, H., Barnes, R. J., & Vanhamäki, H. (2020). Science data products for AMPERE. *Ionospheric multi-spacecraft analysis tools: Approaches for deriving ionospheric parameters*, 141–165.

Weimer, D. R., Mehta, P. M., Licata, R. J., & Tobiska, W. K. (2023). Global variations in the time delays between polar ionospheric heating and the neutral density response. *Space Weather*, *21*(4), e2022SW003410.

Zesta, E., & Oliveira, D. M. (2019). Thermospheric heating and cooling times during geomagnetic storms, including extreme events. *Geophysical Research Letters*, *46*(22), 12739–12746.

Zhou, Y.-L., M. A., S.-Y., Lühr, H., Wang, H., & Dang, G. (2007). Changes of Thermospheric Mass Density and Their Relations with Joule Heating and Ring Current Index During Nov. 2003 Superstorm—CHAMP Observations. *Chinese Journal of Geophysics*, *50*(4), 856–865.

Zhu, Q., Lu, G., Lei, J., Deng, Y., Doornbos, E., van den IJssel, J., & Siemes, C. (2023). Interhemispheric asymmetry of the thermospheric neutral density response to the 7–9 september 2017 geomagnetic storms. *Geophysical Research Letters*, *50*(11), e2023GL103208.